World Academy of Science, Engineering and Technology
International Journal of Civil and Environmental Engineering
Vol:15, No:2, 2021

Research of Strong-Column-Weak-Beam Criteria of Reinforced Concrete Frames Subjected to Biaxial Seismic Excitation

Chong Zhang, Mu-Xuan Tao

***Abstract*—**In several earthquakes, numerous reinforced concrete (RC) frames subjected to seismic excitation demonstrated a collapse pattern characterized by column hinges, though designed according to the Strong-Column-Weak-Beam (S-C-W-B) criteria. The effect of biaxial seismic excitation on the disparity between design and actual performance is carefully investigated in this article. First, a modified load contour method is proposed to derive a closed-form equation of biaxial bending moment strength, which is verified by numerical and experimental tests. Afterwards, a group of time history analyses of a simple frame modeled by fiber beam-column elements subjected to biaxial seismic excitation are conducted to verify that the current S-C-W-B criteria are not adequate to prevent the occurrence of column hinges. A biaxial over-strength factor is developed based on the proposed equation, and the reinforcement of columns is appropriately amplified with this factor to prevent the occurrence of column hinges under biaxial excitation, which is proved to be effective by another group of time history analyses.

***Keywords*—**Biaxial bending moment strength, biaxial seismic excitation, fiber beam-column model, load contour method, strong-column-weak-beam.

I. Introduction

THE philosophy of capacity design has been widely adopted in seismic design of structures. In capacity design, certain structural members are suitably designed and detailed for energy dissipation, and ductile inelastic deformation is allowed to happen in these members. Other members are designed with higher strength to inhibit brittle failure mode of the structure. The capacity design was first proposed and applied in New Zealand in 1960s [1]-[3], and then were quickly accepted all over the world. With respect to its application to RC frames, it requires a specific criteria called S-C-W-B, which ensures the plastic hinges to develop at beam end before at the column end and thus prevent the development of a soft-storey failure mode featured with plastic hinges developing simultaneously at both ends of all the columns in the same storey.

Performance of a great number of RC frames subjected to earthquake excitation, however, has not corresponded to the initial aim of capacity design [4], as observed in the earthquakes in Iran [5], Kashmir [6], Wenchuan [7] and Turkey [8]. Though designed to conforming the rule of S-C-W-B provided in the available design codes [9]-[11], these structures still suffered from a soft storey failure, inducing great loss of life and property. Considering the prevailing of RC frames in civil engineering, it is vital to find the cause of the disparity between design and actual performance.

Several factors have been taken into consideration to account for this disparity. Slab participation, which is carefully studied by [12]-[14], is believed to contribute to the strength amplification of beams and thus results in the minor probability of plastic hinge development in beams. The influence of non-structural infill components was demonstrated by [3] which verified that the non-structural components can make the adjacent columns less slender and more vulnerable to brittle shear failure. The influence of biaxial earthquake excitation, however, has not caught enough concentration. Previous researches [15]-[20] confirmed that frames present more violent response when subjected to biaxial earthquake excitation than uniaxial earthquake excitation, which is known as *biaxial effect*. These researches focused more on the inelastic response of reinforced columns under biaxial excitation and accounted the biaxial effect on the interaction of two directions in stiffness degradation and the following *P-Δ* effect. Li et al. [21] addressed the insufficiency of current column overstrength factor under 45° earthquake excitation but the result was rough since it did not take the column biaxial bending strength into consideration and other incidence directions were not discussed. In general, the underlying weakness of traditional S-C-W-B criteria has not been pointed out and an efficient modification method to address the *biaxial effect* has not been clearly proposed.

For the sake of simplicity in design and construction, a frame is considered irrelevantly as plane structures along its two principal axes and designed neglecting the effect of biaxial earthquake response under most conditions. With respect to the S-C-W-B criteria, however, insecurity may arise from this negligence. On one hand, the flexural moment demand of a column, which equals to the additivity of the moment demand vectors in two principal axes results from the equilibrium with adjacent beams. On the other hand, the flexural strength in a specific direction is not simply adding of the flexural strength in two principal axes. The disparity between design and actual performance may lie in the mismatch of bending moment demand and strength of columns.

In this article, the influence of biaxial earthquake excitation on the criteria of S-C-W-B is carefully analyzed. A more delicate biaxial bending strength model of columns under axial

Chong Zhang is with Department of Civil Engineering, Tsinghua University, Beijing, China (phone: +8613717792690; e-mail: zhangcho19@mails.tsinghua.edu.cn).

Mu-Xuan Tao is with Department of Civil Engineering, Tsinghua University, Beijing, China (phone: +8613810486510; e-mail: taomuxuan@mail.tsinghua.edu.cn).

load is given to introduce the biaxial overstrength factor, α. Time-history analyses are then conducted to obtain the inelastic dynamic response of frames subjected to specific ground excitations. The influence of the biaxial effect on the distributions of plastic hinges is discussed. Subsequently, with the help of α, a modified design method that allows for satisfying the S-C–W-B criterion and preventing the soft storey failure mode under biaxial earthquake excitation was developed.

II. Modelling of Biaxial Overstrength Factor

A. Introduction of Biaxial Overstrength Factor

With respect to a typical rectangular RC column, the bending moment demand induced by biaxial earthquake excitation is illustrated in Fig. 1 (a) as a set of vectors whose ends lie on a rectangular boundary. The shape of the boundary is rectangular because the criteria of S-C-W-B ensure that the component of moment demand in each of the two principal directions never exceeds the bending strength of the adjacent beam in that direction. The boundary of bending strength of columns is shown in Fig. 1 (b), the shape of which is determined by the aspect ratio of the section, the reinforcement arrangement and the material characteristics. The gap between the bending moment demand and resistance of columns can be simply characterized by α , biaxial overstrength factor, defined as:

$$\alpha(\theta) = \min\left\{\frac{M_{\mathrm{cu,x}}}{M_{\mathrm{cu}}(\theta)\cos\theta}, \frac{M_{\mathrm{cu,y}}}{M_{\mathrm{cu}}(\theta)\sin\theta}\right\},\ \theta \in [0, \pi/2] \quad (1)$$

where $M_{\mathrm{cu,x}}$ and $M_{\mathrm{cu,y}}$ represent the bending moment strength in x and y directions, respectively, and $M_{\mathrm{cu}}(\theta)$ is the bending moment strength in direction of θ from x axis. The peak value of α is obtained when $\theta = \arctan(M_{\mathrm{cu,y}}/M_{\mathrm{cu,x}})$. To compute α and apply it in design, a closed-form equation of $M_{\mathrm{cu}}(\theta)$ is required.

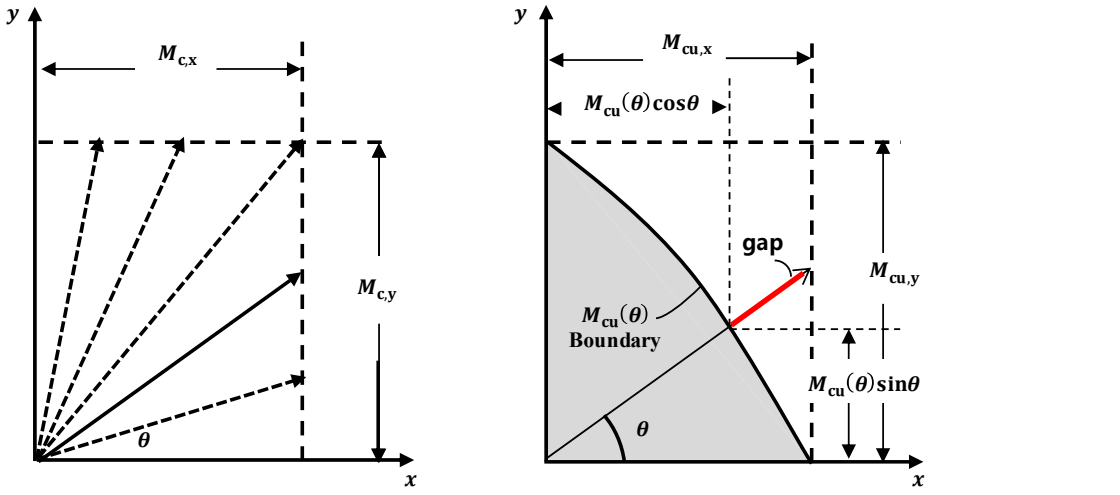

(a) biaxial bending moment demand of columns (b) gap between bending moment demand and resistance of columns

Fig. 1 Illustration of biaxial overstrength factor

The biaxial bending strength of RC columns subjected to axial load has been widely investigated in the literature, and the Eurocode 2 suggests a simplified criterion, a load contour model first proposed by Bresler [22] in 1960:

$$\left(\frac{M_{\mathrm{Edz}}}{M_{\mathrm{Rdz}}}\right)^{a} + \left(\frac{M_{\mathrm{Edy}}}{M_{\mathrm{Rdy}}}\right)^{a} \le 1.0 \quad (2)$$

where M_{Edz} and M_{Edy} are the design moment around the respective axis, M_{Rdz} and M_{Rdy} are the moment resistance in the respective direction, a is the exponent which floats up and down between 1 and 2. A variety of studies [23]-[26] have investigated the dependence relation of this exponent on the material and geometry characteristics of the cross section, utilizing the fiber discretization method. Most of them proposed a closed-form equation of the exponent combining the effect of aspect ratio, the reinforcement percentage and axial load. Usually, however, with too many coefficients to estimate, there remains difficulty in applying these equations to practical engineering. In addition, the aspect ratio is not explicitly included in the original equation. Therefore, the relation between the exponent and other parameters needs to be carefully studied, with more insight involved, and a closed-form equation of biaxial overstrength factor, α, is derived on the basis of it, as discussed in following sections.

B. Derivation of the Ideal Form

RC column members are complicated combination of concrete and steel reinforcement, which results in the difficulty of direct proposal of a closed-form equation. It is reasonable to put RC members aside temporarily and try to find the basic form of the equation from an ideal cross section.

We consider a rectangular and an elliptical cross section made from ideal elastic-perfectly plastic material, as shown in

Fig. 2. Some regular hypotheses adopted are as follows:

- plane sections remain plane after deformation,
- the model is subjected to pure bending, with zero axial force; and,
- the yield strength of the cross section $M(\theta)$ is signified by the first yield of outermost fiber.

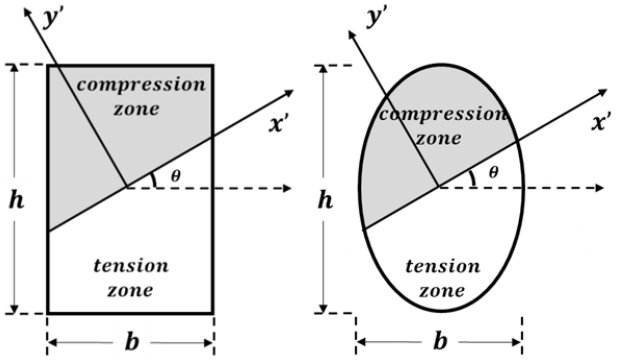

(a) rectangle model (b) elliptical model

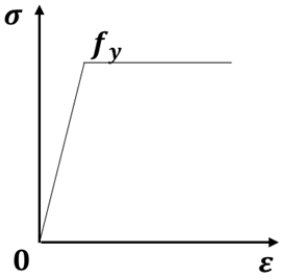

(c) constitutive model of the ideal elastic-perfectly plastic material

Fig. 2 Ideal rectangle and elliptical model

Two theoretical equations of the cross section's yield strength $M(\theta)$ are obtained for the respective rectangle and elliptical model utilizing Mathematica [27]:

$$M_{\text{rect}}(\theta) = M_{\text{rect, x}} \frac{\cos^2\theta + \sin^2\theta / e^2}{\cos\theta + \sin\theta / e} = M_{\text{rect, y}} \frac{e^2\cos^2\theta + \sin^2\theta}{e\cos\theta + \sin\theta},\ \theta \in [0, \pi/2] \tag{3}$$

$$M_{\text{elli}}(\theta) = M_{\text{elli,x}} \frac{\cos^2\theta + \sin^2\theta / e^2}{\left(\cos^2\theta + \sin^2\theta / e^2\right)^{1/2}} = M_{\text{elli,y}} \frac{e^2\cos^2\theta + \sin^2\theta}{\left(e^2\cos^2\theta + \sin^2\theta\right)^{1/2}},\ \theta \in [0, \pi/2] \tag{4}$$

where $M_{\text{rect / elli, x / y}}$ is the yield moment in the respective principal direction for either rectangle or elliptical section, $M_{\text{rect/elli}}(\theta)$ is the yield moment in the direction of x axis rotated by θ and e is the aspect ratio of the cross section, defined by h/b. Further, according to the classical mechanics, $M_{\text{rect, x}} = bh^2 f_y/6$, $M_{\text{rect, y}} = hb^2 f_y/6$, $M_{\text{elli, x}} = \pi bh^2 f_y/32$, $M_{\text{elli, y}} = \pi hb^2 f_y/32$. With e equal to 1, (3) and (4) will degrade into the equations describing square and circle sections, respectively.

Note the similarity between (3) and (4). If they are rearranged in the form of (5), there appears a basic equation with characteristics of a load contour model described above, with an exponent P taking the value of 1 and 2.

$$M(\theta) = M_x \frac{\cos^2\theta + \sin^2\theta / e^2}{\left(\cos^P\theta + \sin^P\theta / e^P\right)^{1/P}} = M_y \frac{e^2\cos^2\theta + \sin^2\theta}{\left(e^P\cos^P\theta + \sin^P\theta\right)^{1/P}},\ \theta \in [0, \pi/2] \tag{5}$$

Several differences, however, still remain between the previous load contour method and this model. Aspect ratio's effect is expressed explicitly in (5), while being included in the exponent's expression in the previous load contour method. Furthermore, in (5), $M(\theta)$ is expressed in the form of polar coordinates instead of combination of $[M_x(\theta), M_y(\theta)]$ in Cartesian coordinates, which is convenient for the transformation into biaxial overstrength factor, α, as (6) shows. The peak value of α is obtained when $\theta = \arctan(1/e)$.

$$\alpha = \min\left\{\frac{\left(1+\tan^P\theta/e^P\right)^{1/P}}{\cos^2\theta+\sin^2\theta/e^2}, \frac{\left(1+e^P\cot^P\theta\right)^{1/P}}{e^2\cos^2\theta+\sin^2\theta}\right\},\quad \theta \in [0, \pi/2] \tag{6}$$

C. Parameter Analysis and Curve Fitting

It is assumed that (5) and (6) also hold for the rectangle RC sections, with the exponent P taking real numbers from 1 to 2 instead of just these two integers. The dependence of P on the geometry, material characteristics and reinforcement placement should be thoroughly investigated, utilizing the fiber discretization model. In fiber discretization model, briefly, the cross section is cut into finite small fibers, and each fiber obeys its own law of constitution depending on whether it is concrete or steel. There exists no mutual compression between fibers. The plain section assumption is conserved for this model.

The model illustration and material properties are shown in Fig. 3. The basic computational process is: 1) give an axial load level, n_{AF}; 2) give a rotation angle θ; 3) assume that the outermost concrete fiber reaches the peak strain ε_0, then calculate the strain at the center, ε, and the curvature of cross section, ϕ under the given n_{AF} and θ; 4) calculate the bending strength M(θ) of cross section; 5) repeat the above procedure to traverse each combination of axial load level n_{AF} and rotation angle θ. Several assumptions are adopted for simplicity and the application in engineering: 1) The top and bottom of the section share the same reinforcement as is also the case for the left and right of the section. The top (or bottom) reinforcement ratio is denoted as ρ_x and the left (or right) reinforcement ratio is denoted as ρ_y. 2) the thicknesses of the covering concrete are the same for each side of the section.

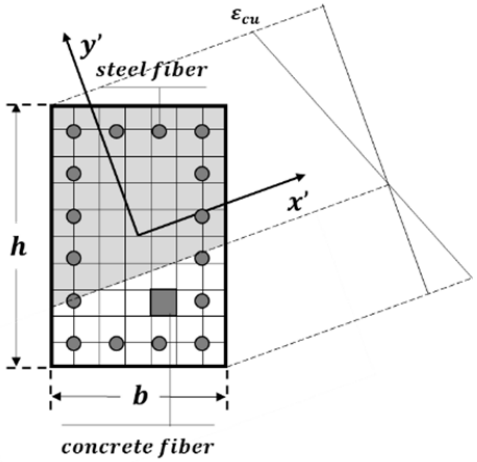

(a) fiber discretization model

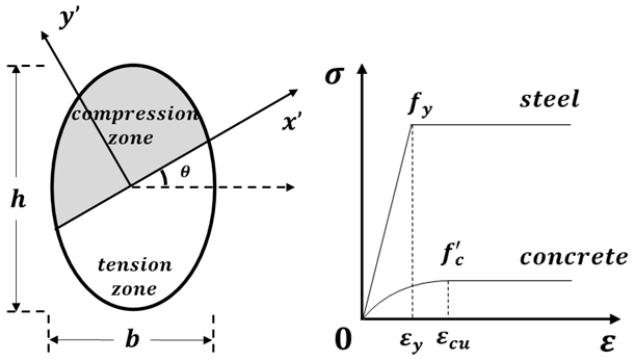

(b) Elliptical model (c) constitutive model of steel and concrete

Fig. 3 Fiber discretization model and material properties

As far as the strain range is concerned in RC column members, elastic-perfectly plastic constitutive model is appropriate for steel reinforcement. To take the constrain effect of transverse reinforcement to concrete into consideration, the *Rüsch* model [28] shown in (7) is selected, which also simplifies the computation. The tensile strength of concrete is neglected.

$$\sigma_c = \begin{cases} f_c' \left[2\dfrac{\varepsilon}{\varepsilon_0} - \left(\dfrac{\varepsilon}{\varepsilon_0} \right)^2 \right] & 0 \le \varepsilon \le \varepsilon_0 \\ f_c' & \varepsilon > \varepsilon_0 \end{cases} \tag{7}$$

To fit an appropriate form of exponent P, it is assumed that the exponent P keeps constant for a specific section. Thus if the peak point of α–θ curve, (arctan(1/e), α_{max}) is precisely captured, the whole curve should be precisely replicated. Numerical analysis shows that n_{AF} is the main variable influencing α_{max} and α_{max}- n_{AF} curves are plotted in Fig. 4. α_{max} first rises up with the increase of n_{AF} and then declines with the increase of n_{AF} after reaching the peak point. As the reinforcement ratio rises, the whole α_{max}- n_{AF} curve shifts to the upper left. The steel yield strength f_y has the same effect on the curve as the reinforcement ratio. The concrete strength f_c' seems to have an opposite but smaller effect on the curve.

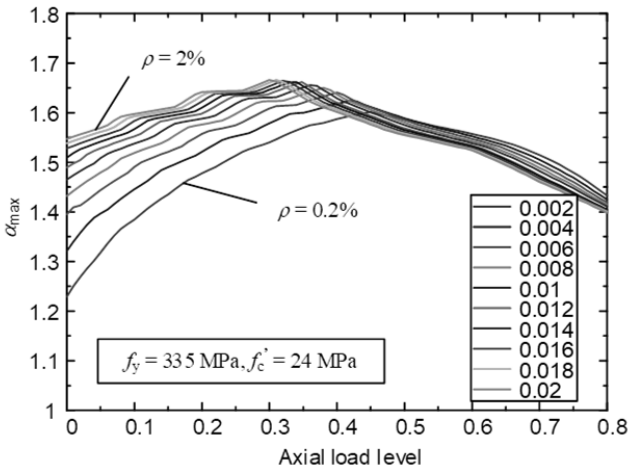

(a) influence of reinforcement ratio

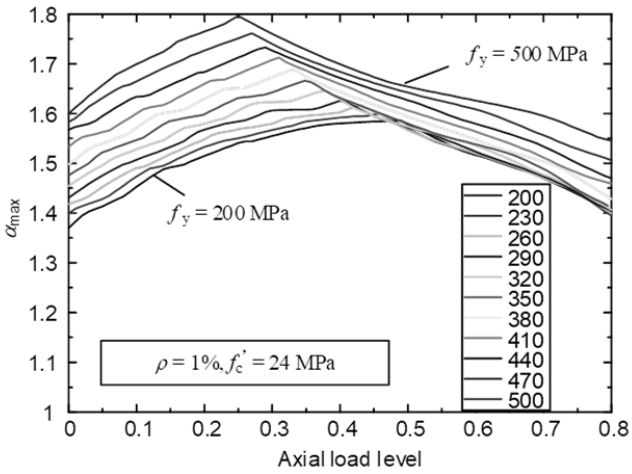

(b) influence of f_y

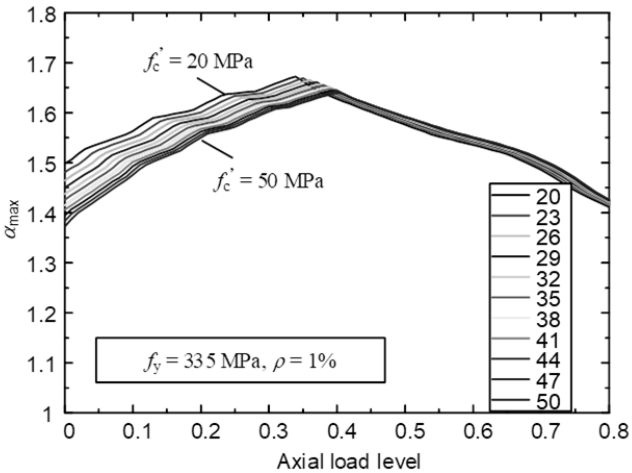

(c) influence of f_c'

Fig. 4 Parametric analysis of α_{max}

The dependence form of α_{max} on n_{AF} can be summarized as a combination of parabolic function and a linear function, as (8) shows. The reason why the equation is written in such a form lies in the characteristic of concrete and steel and their combination. As we know, the bending moment strength of materials like steel has a linear relation with the axial load level since with the increase of axial load level the yield curvature declines. As for concrete, however, a section made of 'ideal' concrete does not have pure bending strength for the 'ideal' concrete cannot bear tensile stress. As the axial load level increases, the yield curvature declines while the non-zero-stress effective zone expands, and the bending strength increases in a parabolic form. After the effective zone has expanded to the whole section, the concrete section's bending strength performs in the same way as the steel section. Combining both materials, the RC section inherits both of their characters without doubt, as is shown in Fig. 5. Thus it is reasonable to assume such a form as (8). If the aspect ratio e is constrained to 1 and ρ_x is equal to ρ_y, the exponent P can be expressed as $P = 1/\log_2(\alpha_{max})$. Then the final equation form of exponent P is obtained, as shown in (9), which is the starting point of curve fitting. As for the case in which aspect ratio e is not equal to 1 or ρ_x is not equal to ρ_y, the definition of the aspect ratio e and ρ are appropriately adjusted to meet the requirement.

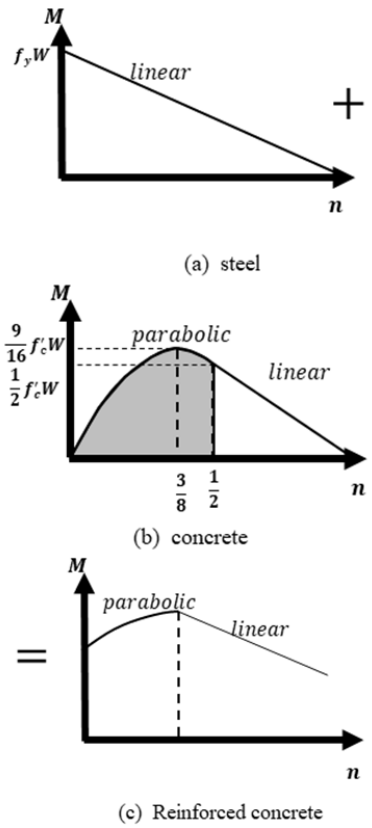

Fig. 5 Illustration of selected fitting function

$$\alpha_{max} = \begin{cases} \beta - k_1(n_{AF} - n_b)^2 & n_{AF} \le n_b \\ \beta - k_2(n_{AF} - n_b) & n_{AF} > n_b \end{cases} \quad (8)$$

$$P = \begin{cases} 1/\log_2\left[\beta - k_1(n_{AF} - n_b)^2\right] & n_{AF} \le n_b \\ 1/\log_2\left[\beta - k_2(n_{AF} - n_b)\right] & n_{AF} > n_b \end{cases} \quad (9)$$

where n_{AF} ranges from 0 to 0.8.

Subjected to the prerequisite that the aspect ratio e is constrained to 1 and ρ_x is equal to ρ_y, a variety of numerical RC sections covering different independent variables f_y, f_c', and ρ ($=\rho_x=\rho_y$) are analyzed to find the dependent relations of the controlling parameters β, n_b, k_1 and k_2 on the independent variables. Results show that, on the whole, there exist linear relations between the dependent and independent variables. Therefore, linear regression is performed to acquire the explicit dependence relations, with results aggregated in (10):

$$\begin{aligned} \beta &= 1.410 + 4.43\rho + 5.679\times10^{-4} f_y \\ n_b &= 0.648 - 7.09\rho - 7.277\times10^{-4} f_y + 0.002 f_c' \\ k_1 &= -0.661 + 0.0072 f_y \\ k_2 &= 0.596 + 4.86\rho - 4.07\times10^{-4} f_y \end{aligned} \quad (10)$$

where ρ ranges from 0.1% to 2%, f_y from 200MPa to 500MPa and f_c' from 20MPa to 50MPa.

D.Verification of Proposed Model by Fiber Discretization Model Analysis and Experimental Tests

To show the accuracy of the curve fitting, a number of numerical sections are calculated to compare the α calculated by equations with α obtained by fiber discretization model analysis. The error is controlled within 10% for all cases and 3% for symmetrical sections, as Fig. 6 (a) shows. These results also verify that the whole curve is perfectly replicated if the peak point is captured by the equation. The fitting equation however is not the final version. When the aspect ratio e is not equal to 1 or ρ_x is not equal to ρ_y, the definition of e and ρ is adjusted to (11) and (12), respectively, according to more fiber discretization model analysis. With this definition, ρ_x and ρ_y are symmetrical in these equations, and when e is equal to 1 and ρ_x is equal to ρ_y, these equations will degrade into the definition of symmetrical sections.

$$e = \frac{h-a}{b-a}\exp\{1.6(\rho_x - \rho_y)\frac{f_y}{f_c'}(1-|n_{AF} - 0.3|)\} \quad (11)$$

$$\rho = \max\left\{\rho_x, \rho_y\right\} \quad (12)$$

To show the accuracy of the final version of proposed model, comprised of (6) and (9)-(12), more fiber discretization model analysis are conducted to compare the α calculated by proposed equations with α obtained by fiber discretization model analysis, as shown in Fig. 6 (b). The error is controlled within 10% for most cases.

The proposed model can be verified not only by fiber discretization model results but also by experiment results. Bresler [22] reported 8 biaxial bending tests of RC columns and

gave a prediction of the eccentric compressive force for each test. The actual eccentric compressive force is denoted as P_u and the predicted one P_i. Bresler gave the value of P_i / P_u in his article, listed in Table I.

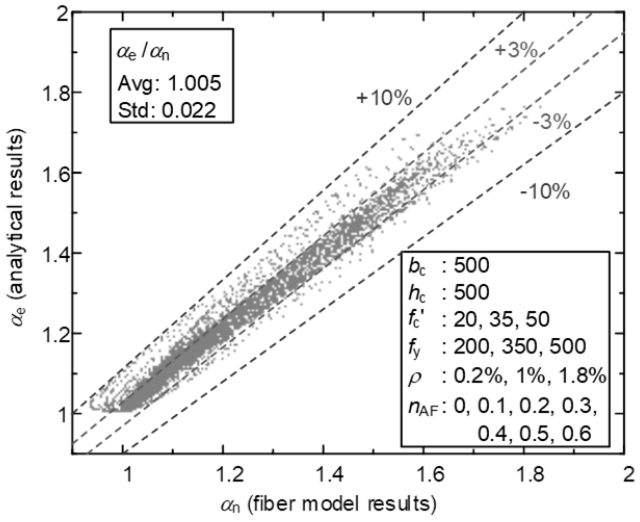

(a) symmetrical sections

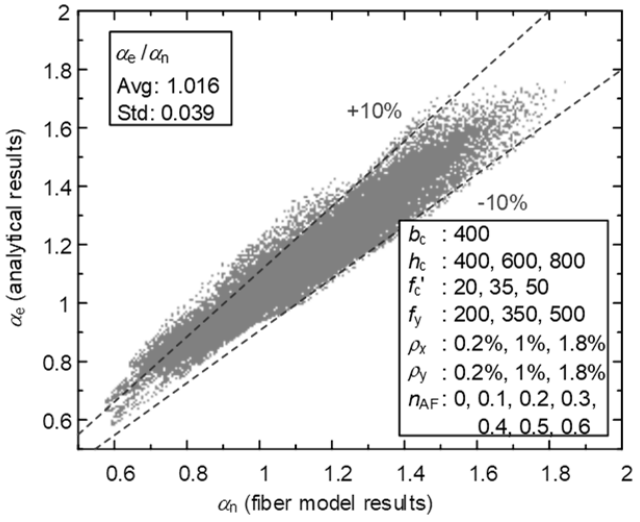

(b) unsymmetrical sections

Fig. 6 Verification of formulas of α for symmetrical sections and unsymmetrical sections

The proposed model of biaxial overstrength factor α in this article, according to (6), can be easily converted to the boundary of bending moment strength, if the bending moment strength in the two principal directions is given. Therefore, in order to compare the proposed model with Bresler's test results, the bending moment strength in the principal directions is first calculated according to the section properties in Besler's article using fiber discretization model. Then the boundary of bending moment strength is calculated using the equations of the proposed model. The difference between the results of proposed model and tests are also listed in Table I and Fig. 7. It is shown that the proposed model is in good agreement with the test results and is more accurate than Bresler's load contour model.

TABLE I
COMPARISON BETWEEN BRESLER'S MODEL AND PROPOSED MODEL

P_i / P_u	Bresler's model	Proposed model
Test 1	0.983	1.069
Test 2	1.063	1.065
Test 3	1.019	0.963
Test 4	0.972	0.996
Test 5	1.103	1.176
Test 6	0.835	1.06
Test 7	0.895	1.038
Test 8	0.9	1.017
Total error $\Sigma\lvert P_i / P_u - 1\rvert$	0.599	0.466

III. RESPONSES OF RC FRAMES SUBJECTED TO BIAXIAL EARTHQUAKE EXCITATIONS

A. Investigated Structure and Its Numerical Model

The biaxial overstrength factor α has been finely modeled and calculated above. In order to verify the effect of it, the influence of biaxial earthquake excitations on RC frame response, mainly the distribution of plastic hinges, have to be investigated first.

A FEM analysis is conducted, in which typical RC frames are modelled using the commercial FE package MSC [29]. Time-history analyses are conducted to obtain the inelastic dynamic response of frames to specific ground excitations and the distribution of plastic hinges is carefully investigated.

The investigated frame has 3 bays in both principal directions and 4 floors. Each bay is 5m long and each floor 4m high. The 3D model and the layout plan of each floor are shown in Fig. 9. The geometry details of the beams and columns are shown in Fig. 10.

Beams and columns are modelled with fiber beam-column element in the subroutine package COMPONA-MARC [30]. The modified fiber beam-column element in the subroutine package COMPONA-MARC has been verified by numerous tests of structural members, sub-structures and structural systems, including monotonic and cyclic loading tests of composite beams, tests of circular and rectangular Concrete Filled Steel Tube (CFST) columns, etc. Uniaxial stress-strain laws of materials are shown in Fig. 8. The skeleton curve of steel is proposed by [31] as shown in Fig. 8 (a), where k_1 = 12, k_2 = 120 and k_3 = 1.2. For the compressive concrete, the stress-strain relationship shown in Fig. 8 (b) is in the form of (7) before the strain reaches the peak strain ε_0 = 2000 με. If the strain exceeds the peak strain, the relationship takes the linear form with the slope ranging from 0 to 0.15 for normal concrete. The stress-strain of tensile concrete takes the form shown in Fig. 8 (c). Concrete has compressive strength f_c'= 24 MPa and the steel reinforcement has tensile and compressive yield strength f_y = 400 MPa.

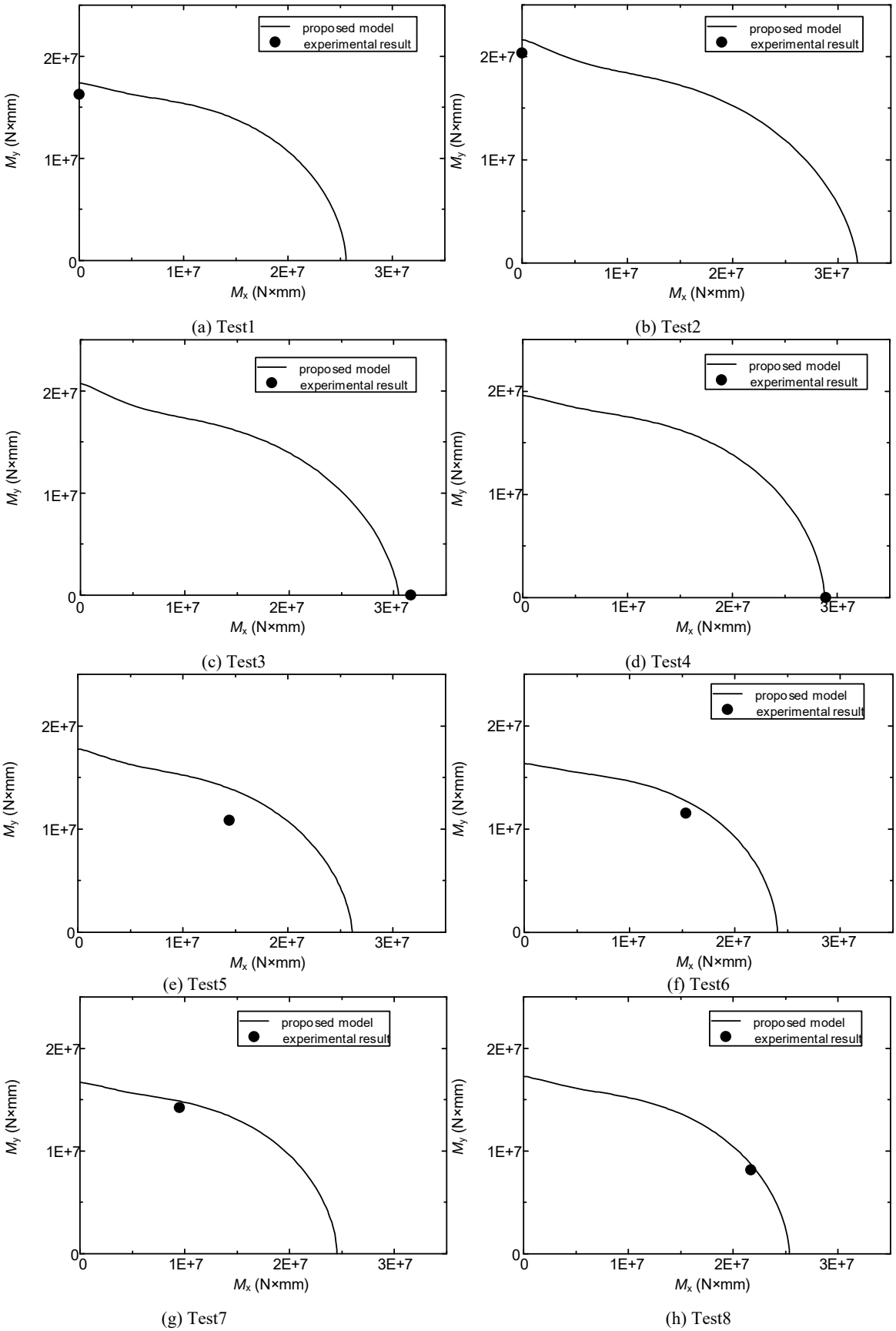

(a) Test1 (b) Test2

(c) Test3 (d) Test4

(e) Test5 (f) Test6

(g) Test7 (h) Test8

Fig. 7 Bresler's test results

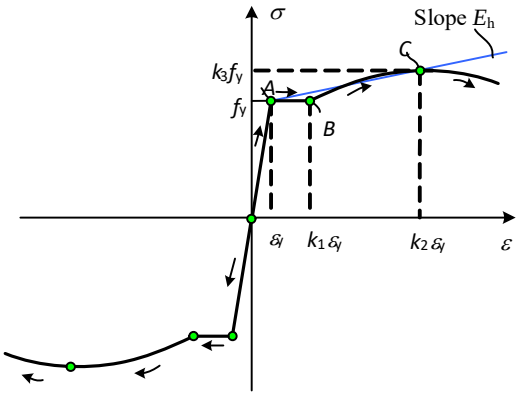

(a) Skeleton Curve of Steel

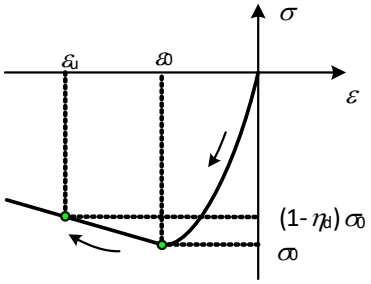

(b) Concrete in compression

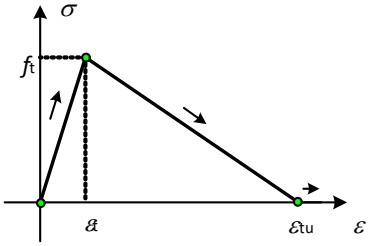

(c) Concrete in tension

Fig. 8 Uniaxial stress-strain laws of steel and concrete

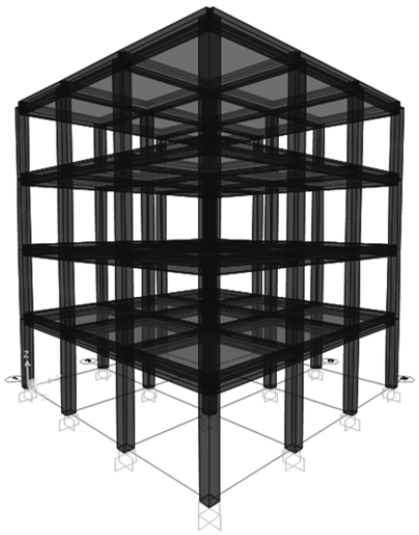

(a) 3D model illustration

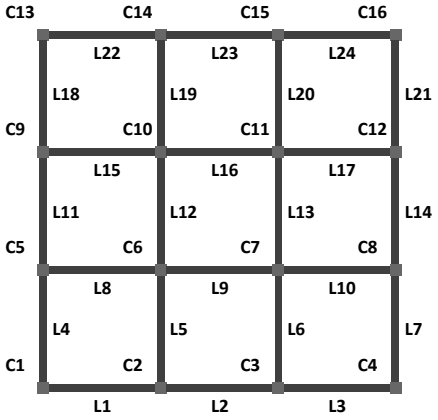

(b) layout plan

Fig. 9 Basic model information

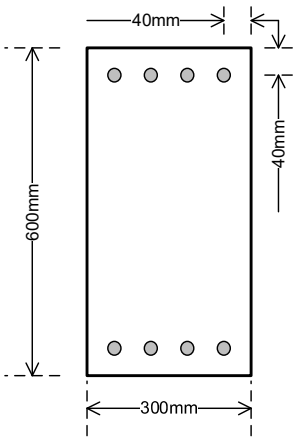

(a) beam details

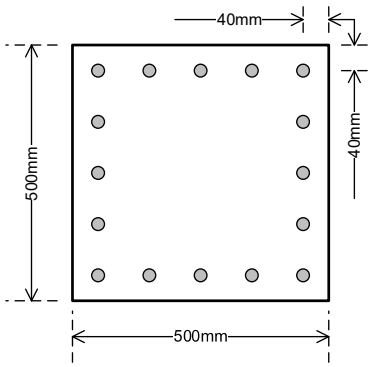

(b) column details

Fig. 10 Component geometry details

In the original FEM model, slab is modelled with multi-layer shell element. The analysis result shows that the effect of slab is mainly to increase the stiffness of the overall frame, which leads to smaller horizontal displacement response when subjected to a specific ground motion wave, compared with the frames without slab modelled. The slab participation effect, which may increase the bending strength of beams, is not clearly observed in FEM analysis. On the contrary, the frames

without slab modeled show fascinating patterns of plastic distribution. Considering that the slab participation is not the main subject in this article, only the response of the frames without slab modelled is investigated and presented in the rest of this article.

The investigated frame is designed precisely according to the Chinese Code for seismic design of buildings (GB50011−2010) [11] which specifies the column bending moment overstrength factor and the beam-column joint equilibrium equation as (13):

$$\Sigma M_{\mathrm{c}} = \eta_{\mathrm{c}} \Sigma M_{\mathrm{b}} \tag{13}$$

where ΣM_{c} and ΣM_{b} are the sum of the resistance moments of the columns and beams framing the joint, respectively, and η_{c} is the column bending moment overstrength factor, taking values of 1.2 and 1.1 in correspondence to the significance level of the frames.

To conduct a time history analysis, appropriate ground motion waves have to be selected. A typical way [32] is to select the waves whose response spectrum fit the design response spectrum best, with great importance attached to two period intervals, $[0.1, T_{\mathrm{g}}]$ and $[T_1 - 0.2\ \mathrm{s}, T_1 + 0.5\ \mathrm{s}]$, where T_{g} is the characteristic site period and T_1 is the fundamental period of the structure. The best fit wave is found by minimizing the MSE (mean square error) between the design response spectrum and the response spectrum of ground motion record after higher weights has been assigned to those two important intervals.

The frame has a fundamental period of 0.65s. The characteristic site period is set to be 0.4s. In correspondence to these parameters, 3 ground motion waves are selected from the PEER Ground Motion Database, denoted by GM1, 2 and 3, as is shown in Fig. 11. Each wave has 2 horizontal components, denoted by H1 and H2. The vertical components are neglected.

B. Classification of Models and Analysis Procedure

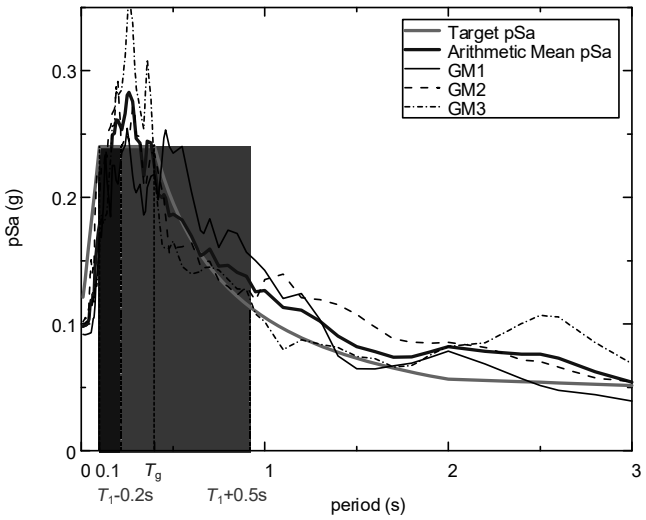

Fig. 11 Response spectrum of selected ground motion waves

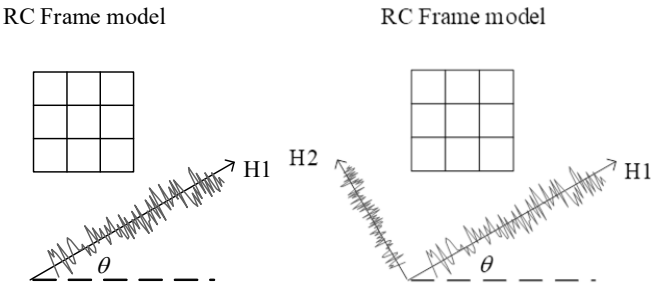

(a) 1 ground motion component (b) 2 ground motion components

Fig. 12 Illustration of excitation type

TABLE II
MODEL CLASSIFICATION

Group ID	Excitation type	Ground motion waves
NS1	single horizontal component	GM1H1
NS2		GM2H1
NS3		GM3H1
ND1	bidirectional horizontal components	GM1H1/H2
ND2		GM2H1/H2
ND3		GM3H1/H2

All the models are classified into different groups by 2 parameters. The first parameter is the excitation type, which is to use only one horizontal component of a wave record in the analysis or to use both of the horizontal components simultaneously, as shown in Fig. 12. Though the latter is closer to reality, the former is easier to deal with and is able to clearly present the nature of biaxial effect. The second parameter is the ground motion waves, and each model is subjected to the 3 selected ground motion waves separately.

The time history analysis is carried out in 2 steps as follows for each group:

i. A model is initially established according to the design result and time history analysis is conducted for a specific ground motion record, with the incident angle, which is the angle between the direction of H1 component and x axis, set to be 0°.
ii. Due to the influence of high-order modes of the frame model to the seismic response, even the requirement of (13) is strictly satisfied in the design; S-C-W-B criteria may still be violated when subjected to ground motions with incident angle of 0°. Therefore, the steel reinforcement area is appropriately adjusted to make sure that no column hinges appear at the incident angle of 0°.
iii. With the model fixed, incident angle is traversed from 0° to 90° by step of 5° and a time history analysis is conducted for each incident angle to acquire the structural responses, mainly including the distribution of plastic hinges and the inter-storey drift angle.

C. Results of Time History Analysis

The code based design of each frame is first tested with ground motion excitation in the principal axes. The maximum inter-storey drift angles of each floor at 0° incident angle are shown in Fig. 13. GM1 ground motion induces the largest inter-storey drift angle, while the responses under GM2 and GM3 are

similar but smaller.

To make sure that no column hinges appear at the incident angle of 0°, the column reinforcement is appropriately amplified, with factors shown in Table III. Then, each group is tested according to the third step. Results show that the first two natural vibration modes are dominant, which are translations along two principal axes, without relative torsion between floors. Column hinge distribution is shown in Fig. 14. Note that column hinges occur when the incident angle is no longer 0 and present with fascinating patterns. In the group NS1, NS2 and NS3, where only one horizontal component of a wave record is used in the analysis, the number of column hinges first increases with the increase of incident angle, reaches the peak at near 45°, and then declines, and at specific incident angles column hinges appear at both the top and the bottom ends of all the columns in the same floor and thus induces a soft storey. In the group ND1, ND2 and ND3, different distribution patterns appear. It seems that there are no explicit relations between the number of column hinges and the incident angle. To explain these messy patterns, it is necessary to look into the mechanism of formation of column hinges.

TABLE III
COLUMN REINFORCEMENT AMPLIFICATION FACTOR

Group ID	Avg. amplification factor
NS1	1.5
NS2	1.09
NS3	1.11
ND1	1.58
ND2	1.39
ND3	1.5

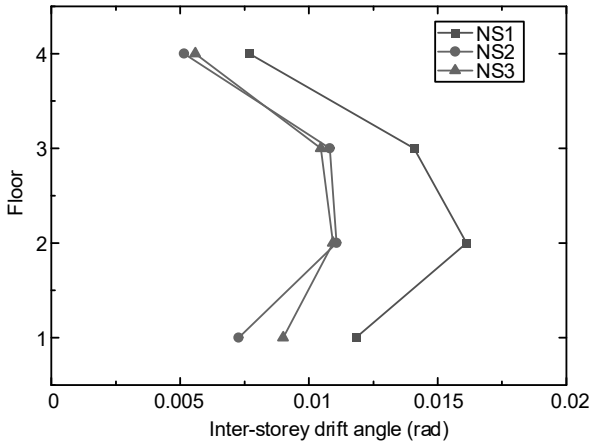

(a) uniaxial input

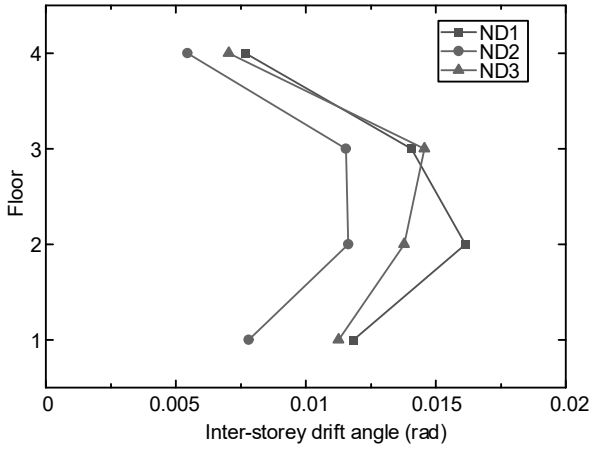

(b) biaxial input

Fig. 13 Inter-story drift angle at 0° incident angle

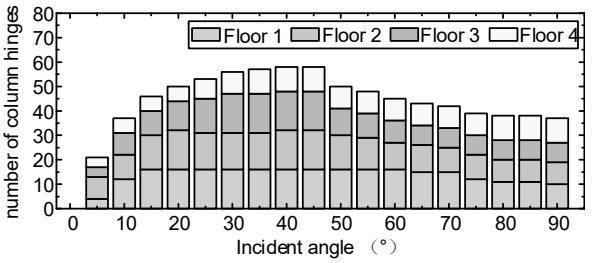

(a) NS1

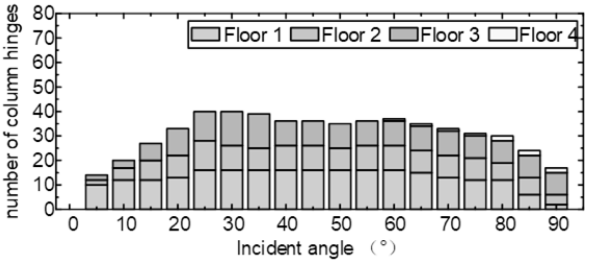

(b) NS2

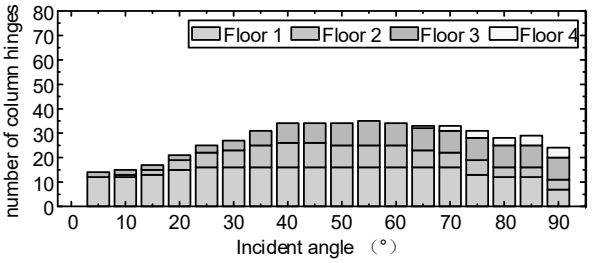

(c) NS3

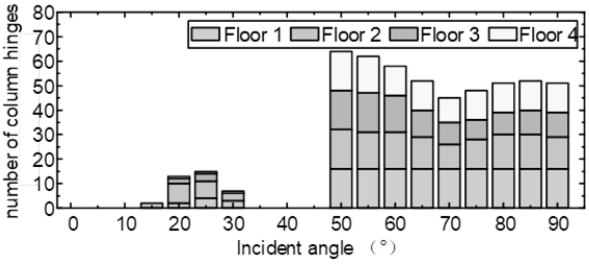

(d) ND1

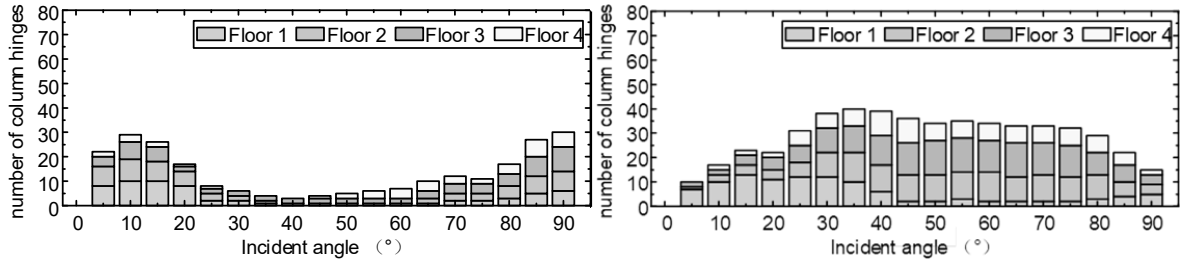

(e) ND2 (f) ND3

Fig. 14 Distribution of column hinges

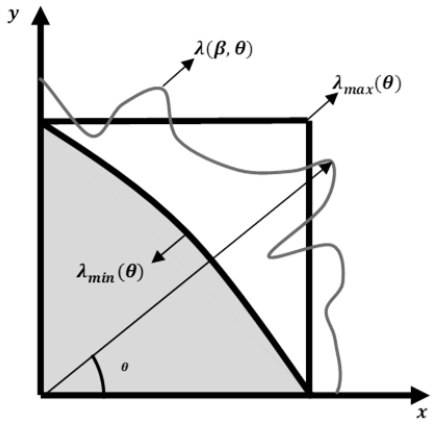

Fig. 15 Mechanism of formation of column hinges

Column hinge is formed when the bending moment $M(\theta)$ at a column end section exceeds the yield moment, $M_{\text{yield}}(\theta)$, where θ is the angle between the bending moment and x-axis. For simplicity it is assumed that the frame has linear stiffness. Thus all kinds of bending moment can be linearly connected to rotation of column end and then the inter-storey floor drift. In Fig. 15 the bending moment of a column $M(\theta)$ is represented with the floor drift $\lambda(\theta\text{-}90°; \beta)$, and the yield moment of a column $M_{\text{yield}}(\theta)$ with $\lambda_{\min}(\theta\text{-}90°)$, using (14):

$$M(\theta) = K\lambda(\theta\text{-}90^\circ;\beta)$$
$$M_{\text{yield}}(\theta) = K\lambda_{\min}(\theta\text{-}90^\circ) \quad (14)$$

where K is the frame stiffness, β is the incident angle and $\lambda_{\min}$ is the minimal inter-storey floor drift to arise the adequate moment in column ends that just reach the yield moment and then form a column hinge. Note that there is a difference of 90° between the angle of bending moment and the angle of the floor drift that causes the bending moment due to the nature of cross product. For simplicity, the pattern of inter-storey floor drift is also plotted in the first quadrant. However, the bending moment demand of column is transported from adjacent beams, so there exists an upper bound for the bending moment, which is also related with the floor drift, $\lambda_{\max}(\theta\text{-}90°)$. For a fixed incident angle, the actual bending moment of a column is represented by

$$M_{\text{actual}}(\theta;\beta) = K\min\left\{\lambda(\theta-90^\circ;\beta), \lambda_{\max}(\theta-90^\circ)\right\} \quad (15)$$

It is reasonable to claim that the larger the actual bending moment is than the yield moment of a specific column, the more possible a plastic hinge forms at the end of the column. In probability language this can be written as:

$$P\{\text{column hinge is formed}\} = f\left(\frac{\min\{\lambda(\theta), \lambda_{\max}(\theta)\}}{\lambda_{\min}(\theta)}\right) \quad (16)$$

where θ now represents the angle between the direction of floor drift and x-axis for simplicity, and f is a specific cumulative probability distribution function, e.g. *Logistic* function. Note that a frame consists of many columns and beams, thus the number of column hinges of the whole frame may be estimated by (17)

$$\mathrm{E}[H(\beta)] = \max_{\theta}\left[\sum_{i=1}^{N} f\left(\frac{\min\{\lambda_i(\theta;\beta), \lambda_{i,\max}(\theta)\}}{\lambda_{i,\min}(\theta)}\right)\right], \quad \theta \in [0, \pi/2] \quad (17)$$

where $\mathrm{E}[H(\beta)]$ is the expectation of the number of column hinges when the incident angle of ground motion is β, index i represents i_{th} column of the frame and N is the total number of columns.

Fig. 16 shows the distribution of the first floor drift, including the direction and value, for each group. In the single-component-ground-motion groups, NS1, NS2 and NS3, a clear picture could be recognized. The direction of maximal floor drift is usually collinear with the direction of ground motion. When the incident angle takes the value of 0°, 90°and 45°, the frame is locked onto the first two natural vibration modes and their combination, respectively, and there appears no other direction of floor drift than the direction of ground motion. Besides, the value of the maximal floor drift corresponding to each incident angle nearly stays the same. In the double-component-ground-motion groups, ND1, ND2 and ND3, however, the direction of floor drift is not directly proportional to the incident angle any more. The direction of maximal floor drift translates with the increase of the incident angle and traverses almost each angle between 0°and 90°. But note that at the incident angle where the number of column hinges is the largest, namely 50° for ND1, 10° for ND2 and 35° for ND3, the

floor drifts of the frame are generally larger and more concentrated near 45° instead of 0°and 90°. In other words, the incident angle may be not important. It is the direction of inter-storey displacement that controls the formation of column hinges.

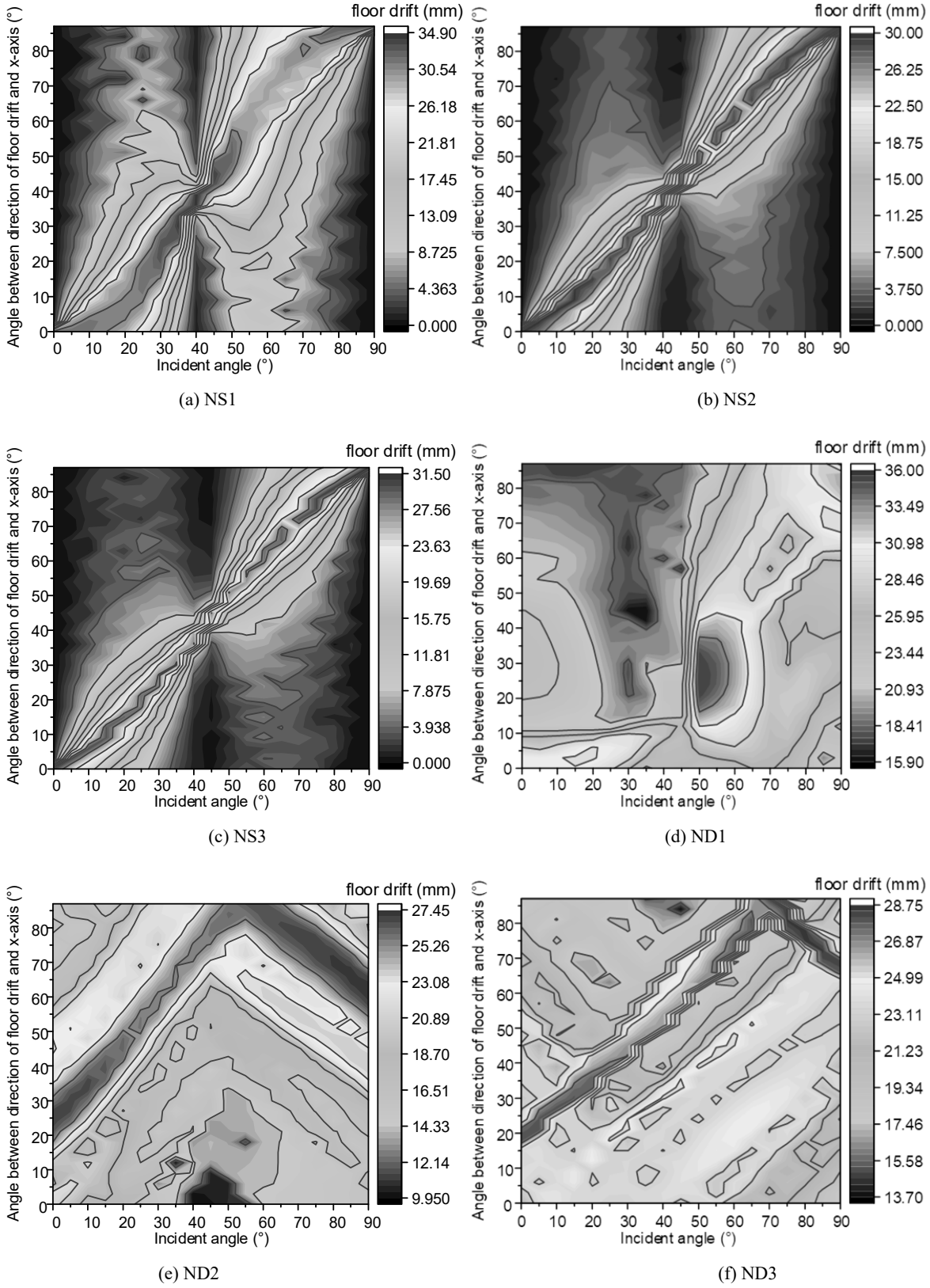

(a) NS1 (b) NS2

(c) NS3 (d) ND1

(e) ND2 (f) ND3

Fig. 16 Distribution of floor drift

In brief, results of time history analysis verify that frame meeting the SCWB rule in the principal axes will develop column hinges and is prone to soft storey failure when subjected to biaxial ground motion. The direction of inter-storey displacement is the essential parameter that controls the formation of column hinges. To make up for this imperfection of design, it is necessary to utilize the biaxial overstrength factor proposed in Section II to amplify the column reinforcement.

IV. Verification of the Effect of Biaxial Overstrength Factor in a Frame Structural System

The biaxial overstrength factor has already been finely developed and verified for individual reinforced column elements. It is essential to verify the effect of the biaxial overstrength factor in preventing the occurrence of column hinges in a frame structural system.

A. Identification of the Direction of Floor Drift and Axial Load Level

According to (6) and (9)-(12), given a column section, the value of its biaxial overstrength factor mainly depends on the direction of the floor drift θ and the axial load level n_{AF}.

Fig. 17 shows a typical pattern of the column axial force in the whole process of ground motion excitation. When the frame is firstly exposed to the dead load, the axial force is larger in the lower floor due to the accumulation of dead load. As for the columns located in the same floor, the axial force is maximal in the central columns, middle in the side columns and minimal in the corner columns. When the frame is subjected to a ground motion, the axial force fluctuates with different amplitudes, and more violently in the lower floors. As for the columns in the same floor, the amplitude of fluctuation is maximum in the corner columns, middle in the side columns and minimal in the central columns. It is not easy to assign a representative value of the axial force because it fluctuates. The axial force induced by the dead load seems an economical choice since it does not need a time history analysis to obtain. The maximum absolute axial force, however, may contain more information about the dynamic response, and it might be convenient to estimate if provided with adequate information about the frame structure and the ground motion excitation. Finally, the maximal absolute axial load level $n_{AF\text{-}max}$ is chosen for the verification process.

The direction of the floor drift, represented by the angle between it and x-axis, θ_v, should be chosen so that in that specific direction the whole frame is the most vulnerable.

According to (17), the most vulnerable direction of floor drift can be determined by

$$\theta_{\mathrm{v}} = \arg\max_{\theta}\left[\sum_{i=1}^{N} f\left(\frac{\min\left\{\lambda_i(\theta;\beta),\lambda_{i,\ \max}(\theta)\right\}}{\lambda_{i,\ \min}(\theta)}\right)\right] \tag{18}$$

It is difficult to solve this equation directly. But things may be easier if several assumptions are made as follows:

i. the ground motion is so intense that $\lambda_t(\theta\ ;\beta)$ is larger than $\lambda_{t,\ \mu\alpha\xi}(\theta\ )$ in all directions, then (18) will degrade into

$$\begin{aligned}\theta_{\mathrm{v}} &= \arg\max_{\theta}\left[\sum_{i=1}^{N} f\left(\frac{\lambda_{i,\ \max}(\theta)}{\lambda_{i,\ \min}(\theta)}\right)\right] \\ &= \arg\max_{\theta}\left[\sum_{i=1}^{N} f\left(\alpha_i(\theta)\right)\right]\end{aligned} \tag{19}$$

ii. the reinforcement in the columns are symmetrical, which means every $\alpha_i(\theta)$ will take the maximum value when $\theta = 45°$.

Therefore, it is reasonable to take the most vulnerable direction of floor drift as 45° temporarily in current analysis.

B. Adjusting of the Reinforcement of the Column by Iteration

After obtaining n_{AF} and $\theta = \theta_v$, it is possible to calculate the biaxial overstrength factor α_θ^0, then the reinforcement of each column should be augmented to make sure that

$$M_\theta^{\mathrm{u}} \geq \alpha_\theta^0 M_\theta^0 \tag{20}$$

where M_θ^{u} is the required bending moment strength to avoid column hinges; and M_θ^0 is the original bending moment strength in the θ direction. However, it is difficult to directly calculate the adequate change of reinforcement to meet (20), thus an iteration process is adopted to calculate it described as:

1) Calculate α_θ^0, M_y^0 (yield moment at y direction) and n_{AF}, set $k_{\mathrm{inc}}^0 = 1$, $k_{\mathrm{tot}}^0 = 1$;
2) For the i_{th} iteration, check if $\left|\alpha_\theta^{i-1}/k_{\mathrm{inc}}^{i-1} - 1\right| < \varepsilon_{\mathrm{tol}}$, if not:

(a). Augment the rebar by $\rho_{\mathrm{x}}^i = \frac{\alpha^{i-1}}{k_{\mathrm{inc}}^{i-1}} \cdot \rho_{\mathrm{x}}^{i-1}$, $\rho_{\mathrm{y}}^i = \frac{\alpha^{i-1}}{k_{\mathrm{inc}}^{i-1}} \cdot \rho_{\mathrm{y}}^{i-1}$, and update $k_{\mathrm{tot}}^i = k_{\mathrm{tot}}^{i-1} \cdot \frac{\alpha_\theta^{i-1}}{k_{\mathrm{inc}}^{i-1}}$;

(b). Recalculate n_{AF}, α_θ^i and M_{y}^i, update $k_{\mathrm{inc}}^i = M_0^i / M_0^{i-1}$;

3) After iteration, output k_{tot} as the final amplification coefficient of rebar where k_{inc} and k_{tot} are coefficients for iteration.

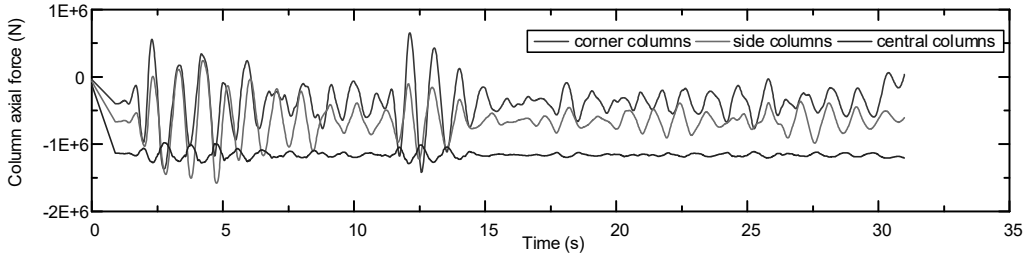

(a) Floor 1

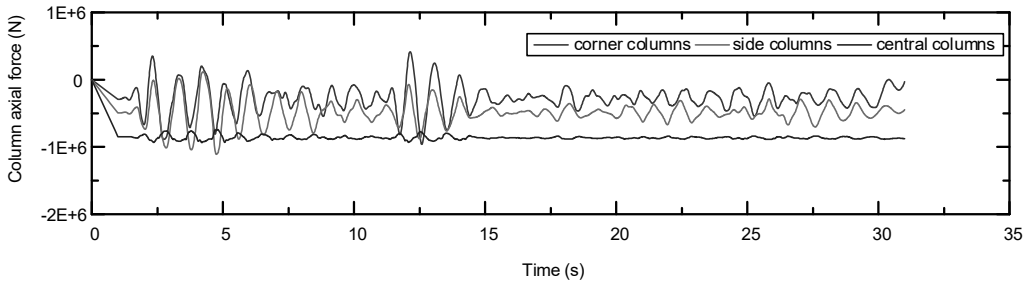

(b) Floor 2

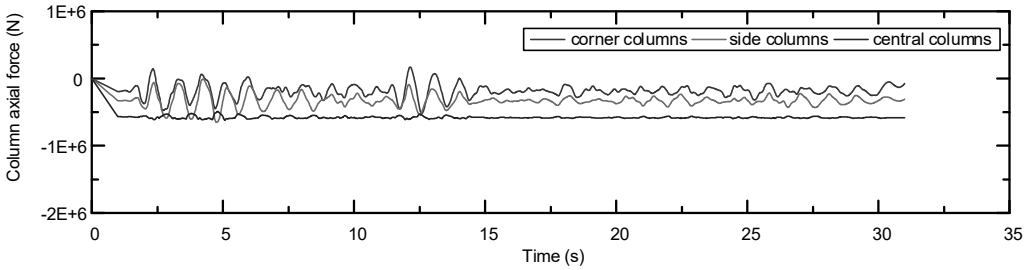

(c) Floor 3

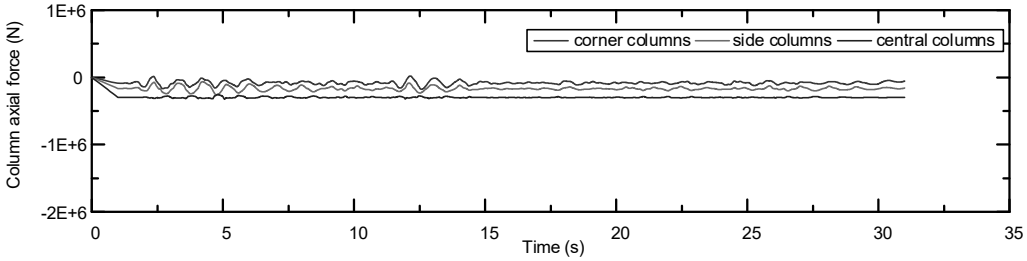

(d) Floor 4

Fig. 17 Column axial force time history subject to GM2

C. Verification by Time History Analysis

We take the numerical model groups ND1, ND2, ND3, NS1, NS2 and NS3 in Table IV for verification. Through the above iteration process, the amplification coefficients for the 64 columns of each frame model are obtained, and Table IV illustrates the maximum, minimum and average values of reinforcement amplification factors of these 64 columns.

The corresponding column hinge results of ND1, ND2, and NS1 are shown in Fig. 18. The number of column hinges is significantly reduced compared to the results before reinforcement amplification. To show that the amplification factors listed in Table IV are necessary, three other time history analyses are conducted with all amplification factors multiplied by a reduction factor 0.9. Results show that numbers of column hinges are reduced, but still larger compared to the results with the original factor. It is then verified that the biaxial overstrength factor is very effective in reducing the column hinges with sufficient accuracy.

For each model in ND3, NS2, and NS3, numbers of column hinges are reduced to zero after the reinforcement is amplified both by α and by $0.9\,\alpha$. For these models, the biaxial overstrength factor is effective but not necessary in reducing column hinges. It is because inter storey floor drifts in these models are not large enough. Thus according to (18), the

comparison between $\lambda_{max}(\theta)$ and $\lambda(\theta;\beta)$ has to be made to determine the most vulnerable direction and may bring about a smaller biaxial overstrength factor.

TABLE IV
COLUMN REINFORCEMENT AMPLIFICATION FACTOR

Group ID	Maximum	Minimum	Average
ND1	2.15	1.51	1.85
ND2	2.09	1.44	1.79
ND3	2.12	1.49	1.84
NS1	2.17	1.51	1.83
NS2	2.11	1.43	1.79
NS3	2.11	1.43	1.79

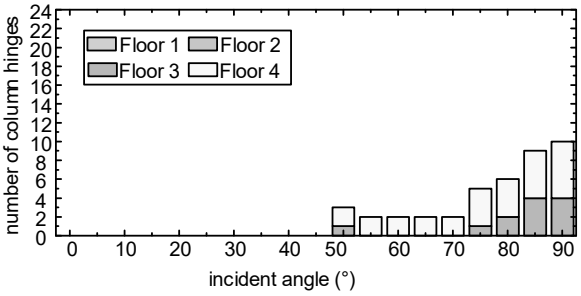

(a) ND1 amplified by α

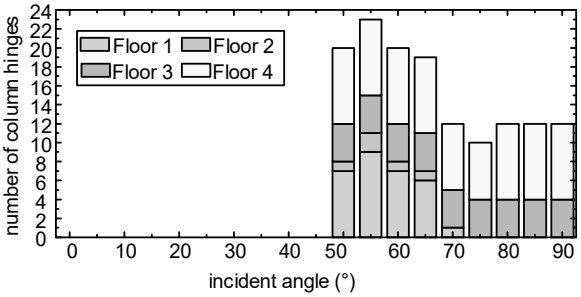

(b) ND1 amplified by 0.9α

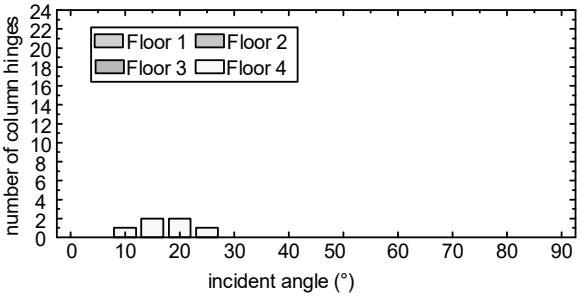

(c) ND2 amplified by α

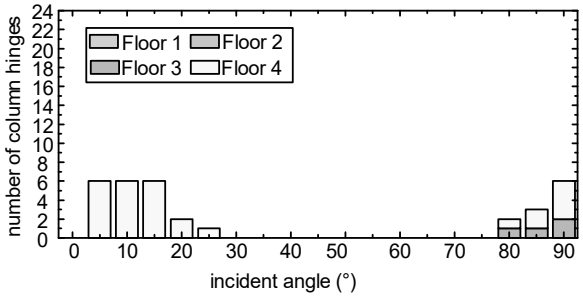

(d) ND2 amplified by 0.9α

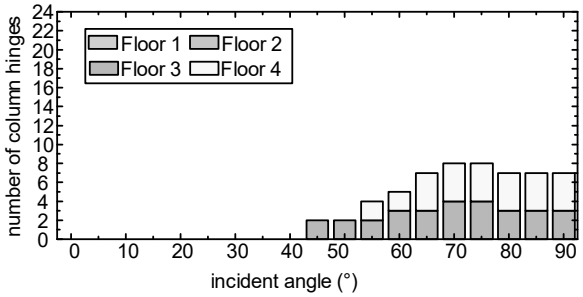

(e) NS1 amplified by α

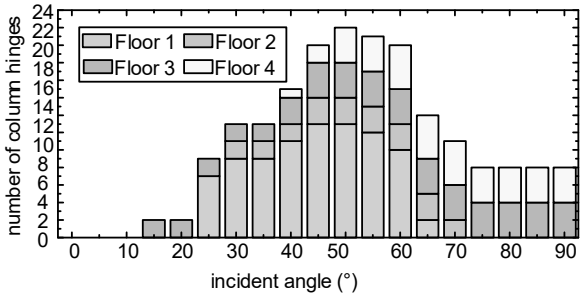

(f) NS1 amplified by 0.9α

Fig. 18 Column hinge distribution after amplification

V. CONCLUSION

In this study, the influence of biaxial earthquake excitation on the criteria of S-C-W-B is systematically analyzed. A closed-form biaxial bending strength equation of columns under axial load is given, on the basis of which the biaxial overstrength factor is proposed. The relationship between the distribution of column hinges and the distribution of floor drifts is carefully investigated by conducting time history analysis of simple frames subjected to ground motion excitation. Finally, the effect of biaxial overstrength factor on reducing column hinges is verified by FEM experiments. The main conclusions are as follows:

(1) Even if the longitudinal reinforcement of columns is appropriately placed to satisfice the bending moment demand in the principal axes, it is difficult to meet the demand in other directions. While the current S-C-W-B criteria are effective in controlling the number of column hinges when the incident angle of ground motion is 0°, it will probably fail when the incident angle is no longer 0°.

(2) The incident angle of ground motion is not the parameter directly controlling the formation of column hinges, but the direction and value of floor drifts.
(3) A closed-form biaxial bending strength model of RC columns is developed on the basis of the prevailing load contour method, but with more insight, and is appropriate for both rectangular and circular columns. The main characteristic parameters controlling the model are the reinforcement ratio, the aspect ratio of section, the axial load level and the material strength. Numerical and experimental results verify the reliability of this model. The formula for biaxial overstrength factor is then developed based on this biaxial bending strength model.
(4) After increasing the rebar in the columns with biaxial overstrength factor of about 1.5-2.2, column hinges are significantly reduced and the soft-story mode is prevented.

The time history analysis also shows that the formation of column hinges is not a single structural component behavior but is determined by the overall frame characteristic. More delicate explanation could be put forward only if more attention is concentrated on the overall frame system performance. Slabs play an important role in the dynamic response of frames. However, the influence of slab is not included in the scope of this study, but will be discussed in the follow-up study. The final verification part shows that the complete assurance of S-C-W-B may require an increase by up to 100% in column reinforcement, which is quite uneconomic. Therefore, the follow-up study will focus on the performance-based design with respect to S-C-W-B criteria.

ACKNOWLEDGMENT

The writers gratefully acknowledge the financial support provided by the National Natural Science Foundation of China (Grant No. 51878378).

REFERENCES

[1] J. A. Blume, N. M. Newmark, and L. H. Corning, "Design of multistory reinforced concrete buildings for earthquake motions", Skokie, ILL: *Portland Cement Association*, pp. 318, 1961.
[2] J. P. Hollings, "Reinforced concrete seismic design", *Bull New Zealand Soc Earthq Eng*, vol.2, no. 3, pp. 217-250, 1969.
[3] T. Paulay, and M. J. N. Priestley, "Seismic design of reinforced concrete and masonry buildings", *Wiley*, 1992.
[4] N. Ning, W. J. Qu, and Z. G. J. Ma, "Design recommendations for achieving ''strong-column-weak beam" in RC frames", *Engineering Structures*, vol. 126, pp. 343–352, 2016.
[5] M. Ahmadizade, and H. Shakib, "On the December 26, 2003, southeast Iran earthquake in Bam region", *Engineering Structures*, vol. 26, pp. 1055–70, 2004.
[6] T. Rossetto, and N. Peiris, "Observations of damage due to the Kashmir earthquake of October 8, 2005 and study of current seismic provisions for buildings in Pakistan", *Bull Earthquake Eng*, vol. 7, pp. 681–899, 2009.
[7] B. Zhao, F. Taucer, and T. Rossetto, "Field investigation on the performance of building structures during the 12 May 2008 Wenchuan earthquake in China", *Engineering Structures*, vol. 31, pp. 1707–23, 2009.
[8] M. H. Arslan, and H. H. Korkmaz, "What is to be learned from damage and failure of reinforced concrete structures during recent earthquake in Turkey?", *Engineering Failure Analysis*, vol. 14, pp. 1–22, 2007.
[9] Euro code 8. Design of Structures for Earthquake Resistance-Part1: General rules, seismic actions and rules for buildings. Bruxelles, 2004.
[10] ACI 318-14. Building code requirements for structural concrete, American Concrete Institute, Farmington Hill, 2014.
[11] GB50011-2010. Chinese Code for seismic design of buildings, Beijing, 2010.
[12] S.J. Pantazopoulou, and C.W. French, "Simple analytical model for T-beams in flexure", *Journal of Structural Engineering*, vol. 114, no. 7, pp. 1507-1523, 1988.
[13] S. J. Pantazopoulou, and C.W. French, "Slab participation in practical earthquake design of reinforced concrete frames", *ACI Structural Journal*, vol. 98, no. 4, July-August 2001.
[14] C. W. French, and A. Boroojerdi, "Contribution of R/C floor slabs in resisting lateral loads", *Journal of Structural Engineering*, vol. 115, no. 1, pp. 1-18, 1989.
[15] N. C. Nigam, "Inelastic interactions in the dynamic response of structures", Doctoral dissertation presented to California Institute of Technology, 1967.
[16] R.Padilla-Mora, and W. C. Schnobrich, "Non-linear response of framed structures to two-dimensional earthquake motion", Structural research series No.408, 1974, UILU-ENG-74-2015.
[17] M. I. H. Suharwardy, and D. A. Pecknold, "Inelastic response of reinforced concrete columns subjected to two-dimensional earthquake motions", Structural research series No.455,1978 UILU-ENG-78-2022.
[18] H. Takizawat, and H. Aoyama, "Biaxial effects in modelling earthquake response of R/C structures", *Earthquake engineering and structural dynamics*, vol.4, pp. 523-552, 1976.
[19] A. E. Aktan, and D. A. W. Pecknold, "Effects of two-dimensional earthquake motion on a reinforced concrete column", Structural research series No.399, 1978 UILU-ENG-73-2009.
[20] H. Rodrigues, A. Furtado, and A. Arêde, "Behavior of rectangular reinforced-concrete columns under biaxial cyclic loading and variable axial loads", *Journal of Structural Engineering*, vol. 142, no. 1, 04015085, 2016.
[21] Z. B. Li, C. Y. Liu, and H. Ma, "Damage Mechanism Research on Reinforced Concrete Spatial Joints Subjected to 45-degree Direction Cyclic Loading", *Journal of Beijing university of technology*, vol.37 no.7, 2011 (in Chinese).
[22] B. Bresler, "Design criteria for reinforced columns under axial load and biaxial bending", *ACI Journal*, vol.32, no.5, Nov, 1960.
[23] G. Monti and S. Alessandri, "Assessment of RC columns under combined biaxial bending and axial load", Proceedings of the second fib congress at Naples, Italy, 2006.
[24] H. G. Kwak, and J. H. Kwak, "An improved design formula for a biaxially loaded slender RC column", *Engineering Structures,* vol. 32, pp. 226–237, 2010.
[25] M. Fossetti, and M. Papia, "Dimensionless analysis of RC rectangular sections under axial load and biaxial bending", *Engineering Structures*, vol. 44, pp. 34–45, 2012.
[26] M. D. Stefano, and G. Faella, "An evaluation of the inelastic response of systems under biaxial seismic excitations", *Engineering Structures*, vol. l, no. 9, pp. 724-731, 1996.
[27] Wolfram Research, Inc., Mathematica, Version 11.3.
[28] H. Rüsch, "Research toward a general flexural theory for structural concrete", *ACI Structural Journal*, pp. 1-28, July, 1960.
[29] MSC.Marc Version 2015. MSC.Software Corp., Santa Ana, CA.
[30] M. X. Tao, and J. G. Nie, "Element mesh, section discretization and material hysteretic laws for fiber beam–olumn elements of composite structural members". *Materials and Structures* vol. 48, no. 8, pp. 2521–2544, 2015.
[31] A. Esmaeily, Y. Xiao, "Behavior of reinforced concrete columns under variable axial loads: analysis", *ACI Structural Journal*, vol. 102, no. 5, pp. 736–744, 2005.
[32] Z. Qu, L.P. Ye, P. Pan, "Comparative study on methods of selecting earthquake ground motions for nonlinear time history analyses of building structures", *China Civil Engineering Journal*, vol.44, no.7, 2011 (in Chinese).